LASER-MANUFACTURED MAGNETIC MICROCHIPS FOR EXOSOME ISOLATION AND PATTERNING

John H. Molinski, Siddhant Parwal, and John X.J. Zhang
Thayer School of Engineering, Dartmouth College, Hanover, NH

2024 IEEE 37th International Conference on Micro Electro Mechanical Systems (MEMS) | 979-8-3503-5792-9/24/$31.00 ©2024 IEEE | DOI: 10.1109/MEMS58180.2024.10439482

ABSTRACT
We report the development of a laser-based micromagnet patterning process and magnetic microchip architecture enabled by this process which facilitates isolation of exosomes via pattering of magnetic composite. The laser-based manufacturing process supports raw material to device manufacturing in <30 minutes and enables patterning with microscale lateral resolution (<50 μm), high throughput (400 mm/s), and over large areas (>in^2), without lithographic processing. Using finite element analysis (FEA), we have further optimized individual micromagnet unit cells, resulting in a geometry that was implemented within exosome capture studies. The magnetic microchip architecture introduced herein, consisting of fluid-invasive micromagnets, enables the generation of high magnetic gradient fields throughout the fluid medium rather than confined to the channel walls within standard microfabricated magnets, showing >80% capture efficiency from simulation and on micromagnet exosome patterning.

KEYWORDS
Immunomagnetic capture, magnetic micropatterning, exosomes, laser fabrication

INTRODUCTION
Exosomes are small (30-150 nm) vesicles with important functions in cell-to-cell communication and have been demonstrated to carry an assortment of host-cell specific cargo including microRNA, DNA fragments, and proteins which has propelled their investigation within diagnostic and therapeutic applications [1]. The gold standard technique utilized for their isolation is ultracentrifugation, a timely and labor-intensive process associated with low yields and product purity [2]. Microchip methods, often using immunoaffinity means for capture have become a largely explored alternative, however mass transfer limitations imposed by exosome size along with flow stagnation near microchip walls limits capture efficiency [3]. As such, to further probe the underlying biological functions of exosomes or inform their use within diagnostic or therapeutic applications, methods for their efficient isolation and processing are direly needed.

Microchip-mediated exosome capture has been an intriguing advance within the field, allowing for high exosome purity and yield relative to ultracentrifugation [4]. To further improve capture efficiency and yield, patterning within microchannels has become an increasingly utilized approach that aims to induce turbulent mixing or improve nanoscale mass transfer, promoting interactions between exosomes and capture regions [3], [5], [6]. These devices, however, rely solely on changes of the fluidic environment without the use of external forces; this often results in a significant reduction to flow rates to enable device operation (<1 mL/hr) and limits their clinical utility.

In this paper, we present a microchip fabrication method that allows for the patterning of micromagnets agnostic to pattern geometry and at microscale lateral resolution. We demonstrate through simulation that this microchip configuration, consisting of rationally designed fluid-invasive micromagnets, can enhance capture efficiency due to dual modulation of microscale magnetic fields and the fluidic environment. As a demonstration and a proof-of-concept experiment, we have employed the optimized magnetic microchip for the rapid capture and patterning of exosomes directly from solution, a result that could have important application within fundamental exosome biology, exosome-based diagnostics, and exosome-based therapeutics alike.

MATERIALS/METHODS
Magnetic microchip fabrication: The laser-based fabrication process is a combined laser-ablation and peeling process, which utilizes a magnetic elastomer composite (magPDMS, 50:50 w/w Fe_3O_4 and PDMS) as the micromagnets composition. Firstly, magPDMS components are manually mixed, desiccated, and spread on a substrate to the desired thickness using a two-step blade coating process (KTQ-II adjustable fabricator, 10 μm precision). The first pass evenly distributes the viscous composite whereas the second finely tunes thickness to desired height (in this study 35 μm) where it's then cured rapidly on a hotplate at 150°C (<10 minutes). The magnetic nanoparticles, aside from imbuing magnetic properties within the composite, act dually as an absorber that enables laser ablation. A Technifor Laser Marking Machine (LW1, Gravotech) equipped with a 532-nm Diode Pump Solid State (DPSS) laser was used for all patterning and laser parameters were optimized for a given thickness of the magPDMS layer, or occasionally for a given micromagnet geometry, by controlling speed (mm/s), power (%), DPI, and number of layers. Following laser ablation, the excess areas could easily be peeled away using tweezers. Finally, the fabricated micromagnets were mechanically stabilized using a solution-based dip-coating treatment with Al_2O_3, optimized to form a nanoscale thick coating (~100 nm), and a microwell placed above forming a fluidic cell. Optical characterization of micromagnets was completed using a digital microscope (Keyence VHX-7000 series).

Immunomagnetic exosome capture: Biotinylated human (CD9, CD81, CD63) were purchased from BioLegend and used without further modification. Streptavidin-coated iron oxide nanoparticles (500 nm diameter) were purchased from Luna Nanotech, and prior to use, beads were washed twice within a magnetic stand using 1X PBS. For antibody conjugation to magnetic nanoparticles, a previously optimized ratio of magnetic nanoparticles to antibody (175 μg nanoparticle to 1 μg antibody) was incubated with mixing for 1 hour at room temperature. Conjugated beads were then separated within a magnetic stand and washed

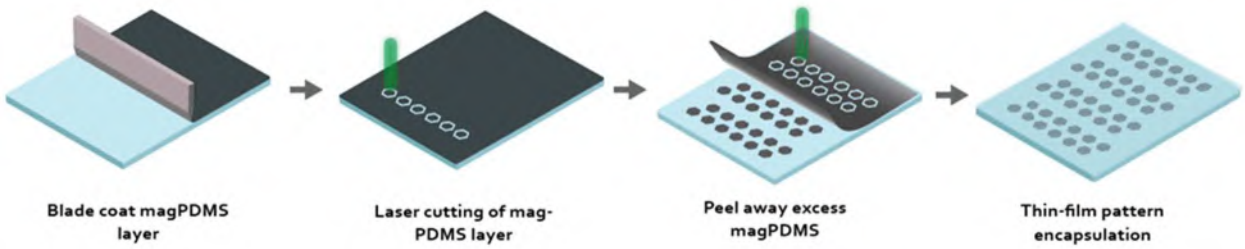

Figure 1: Laser-based micromagnet fabrication. *Schematic for the laser-based fabrication and patterning of micromagnets. Following the last step, the micromagnets can either be integrated with a microwell or encapsulated with a microchannel and can form a multifunctional platform upon which microchip-based systems can be developed.*

twice with PBST (PBS + 0.1% Tween-20) and beads were either used immediately or stored at 4ºC until use. For exosome labeling, plasma was thawed in a 37˚C water bath for 15 min. 200 µL of clinical plasma was incubated with 0.2 µg of antibody for 2 hours at room temperature. Processed plasma samples were finally reconstituted to a final volume of 200 µL with 0.1% BSA in PBST.

Multiphysics simulations: Modeling of particle capture within patterned devices was completed using a customized MATLAB-based FEA workflow. We sought to utilize this model to optimize both micromagnet design and investigate particle dynamics as it interacts with micromagnets within the device. The simulation workflow is as follows: (1) microscope images of the fabricated micromagnet geometries, rather than the idealized geometries were processed and used as MATLAB model inputs. (2) Two separate MATLAB models, one for computational fluid dynamics (CFD) analysis (CFDTool) and another for magnetostatic analysis (FEATool) were generated. Due to the micromagnet symmetry in the Z-direction, CFD simulations were completed in 2D, whereas magnetostatic simulations were completed in 3D. (3) To map over the 2D fluid simulation the magnetic field was averaged over the height of the micromagnet resulting in a 2D mapping of the 3D magnetic field. Since CFD simulations inherently provided velocity vector components $\vec{v}_{f,x}$ and $\vec{v}_{f,y}$ the data did not need further processing. However, for magnetostatic simulations, magnetic field components were first converted to magnetic force components ($\vec{F}_{m,x}$ and $\vec{F}_{m,y}$) where $\vec{F}_m=(m\cdot\nabla)B$, followed by obtaining the velocity of the particle under the influence of both forces, $\vec{v}_p=(\mathbf{1}/6\pi\eta R)(\vec{F}_m+\vec{v}_f)$, where the first term can be recognized as the magnetophoretic particle velocity. (4) Given that the particles velocity is a function of both the magnetophoretic particle velocity and that of the fluid, we expand it component wise as is solved for within the MATLAB model, to obtain the particles component velocities at any given point obtaining $\vec{v}_{p,x}=\vec{v}_{m,x}+\vec{v}_{f,x}$ and $\vec{v}_{p,y}=\vec{v}_{m,y}+\vec{v}_{f,y}$ (see Figure 3). (5) A scaling parameter applied to the magnetic term was incorporated to enable investigation into different operational regimes (ratios of drag force to magnetic force).

In contrast to standard particle trajectory models, which consider lateral deflection of particles within a long, narrow microfluidic channel [7], the presented MATLAB modeling workflow has been optimized to consider the specific device configurations presented, i.e., those which contain flow-invasive magnetic micromagnets. As such, we used this to explore changes in the micromagnet geometry and size as it relates to capture efficiency and defined critical design parameters to enable future development of this class of devices.

Capture characterization: Exosome visualization and detection was completed using a DiD lipid membrane stain (Invitrogen, Ex./Em. 644/665 nm), prepared by mixing 25 mg of DiD in 4 mL of dimethyl sulfoxide. Staining of exosomes was completed with a 15-minute incubation at 37˚C followed by washing of the sample twice with PBST with 0.1% BSA. Imaging was completed with an Andor W1 Spinning Disc confocal microscope under brightfield and fluorescence at 637 nm excitation. Images were processed within the NIS Elements Workstation or Fiji ImageJ.

RESULTS

Laser-assisted micromagnet fabrication: In this manuscript, we present a novel fabrication method for the patterning of fluid-pervasive micromagnets. Figure 1 presents a schematic for the developed fabrication process, which utilizes no specialized equipment or lithographic processing, and is suitable for scaling to meet mass-scale production standards. Using this process, we have demonstrated the feasibility to pattern various micromagnet geometries and have successfully fabricated arrays at large scale (>1 in^2) with microscale lateral resolution (<50 µm). Through experimentation, it was found that several laser parameters altered resolution, including laser power, number of layers, and laser working distance (beam width). Thus, for the given micromagnet thickness of 35 µm, optimized parameters were found to be 2% power, a working distance of 194 mm (which enabled a beam width and pattern fidelity of ~18 µm), and speed of 400 mm/s. Figure 2 shows resolution testing of a basic square geometry, as a function of pattern size (% of 200 x 200 µm) and number of layers, for a fixed frequency and laser power. As can be seen, by increasing the number of layers, fidelity of the pattern increased, but also changed size, an unexpected, but potentially useful facet that allows for greater tunability in pattern geometry and size.

Computational modeling for micromagnet geometry optimization: Particle capture within micromagnet patterned devices occurs when magnetic particles interact with a 'capture region' generated by the fluid-invasive micromagnets, resulting from near-field high gradient

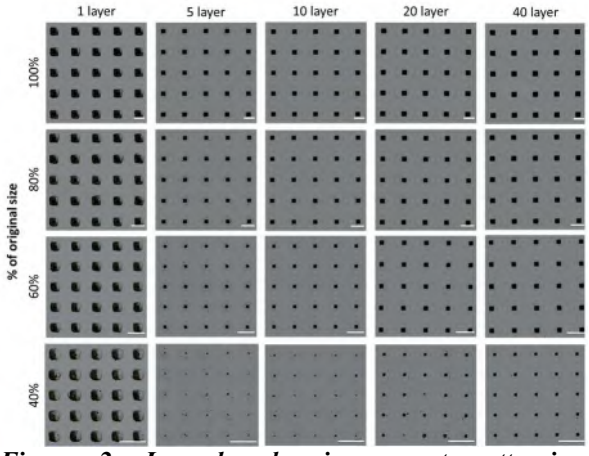

Figure 2: Laser-based micromagnet patterning optimization and resolution. *To determine minimal resolution for laser-based patterning, we reduced a starting pattern size of 200 x 200 µm to 80%, 60%, and 40% of its original size. For all patterning, 2% laser power, 400 mm/s, a pulse frequency of 30 kHz, and working distance of 194 mm was used. All scale bars are 250 µm.*

fields imposing significant magnetic forces on nearby particles. This magnetic force results in a transverse particle velocity which pulls particles across fluid flow streamlines and towards elements where they are immobilized, given magnetic forces are greater than drag forces at the point of capture. This force balance between the drag force and magnetic force dictates captures regions generated by micromagnets and highlights potential influence of pattern design on capture regions. In contrast to standard immunomagnetic capture systems which utilizes only external magnets or thin film micromagnets in which particles need to be positioned nearby to channel walls (typically completed using small microchannel heights or widths or particle focusing), in our system particles need only be nearby patterned micromagnets which are patterned throughout the fluid medium. Through rational design of micromagnets, we can additionally modulate fluid flow, promoting particle movement towards capture regions and further expanding capture region size.

Modeling particle capture utilized a unit cell approach to gauge particle dynamics near to single micromagnet elements. This workflow aimed to give specific and actionable capture efficiency information regarding unit cell design whilst giving a suitable approximation for particle behavior within an array of like elements. In fact, it's expected that the unit cell approach will typically underestimate capture efficiency due to the dense array of and interplay between micromagnet elements within the final device geometry. Results from the simulation workflow are shown in Figure 3 where we first demonstrate particle velocity vectors (top row) as they interact with micromagnets and are under the influence of both magnetic and fluidic forces. Secondly, we convert this vector field to particle streamlines and predict particle capture with each micromagnet geometry (Figure 3, bottom row).

In practice, to simplify simulations and explore the most stringent capture scenario case, we consider capture of a

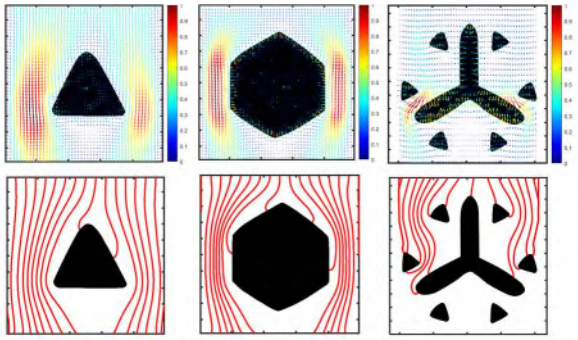

Figure 3: Micromagnet Multiphysics modeling *Micromagnet patterns of varying geometry shown L to R (triangle, hexagonal, and Y-shape). Top row shows results from integrated CFD and magnetostatic simulations within a vector-based plot. Each points represents the direction and normalized velocity of a magnetic particle of 500 nm within flow. Bottom row shows particle streamlines as particles pass micromagnets. Streamlines that terminate at the micromagnet indicate those that have been captured.*

single magnetic particle, given that the magnetic force will only increase with the level of magnetic tagging. We then sought to define a capture area metric, defined as regions where magnetic force dominates drag forces that would allow us to rapidly screen micromagnet geometries for capture, results of which are shown in Figure 4.

Exosome capture using optimized micromagnets:
For initial testing, we developed a simple microwell system, consisting of glass slide substrate patterned with encapsulated micromagnets within a microwell, which were magnetized by a single external magnet (1"x1", N52, KJ Magnetics). From simulation results, we chose the Y-shape geometry for capture studies due to the high capture area ratio generated. Exosomes within undiluted plasma were magnetically tagged with biotinylated pan-exosome markers (CD9, CD63, CD81), as previously described, followed by introduction of plasma (200 µL) within the microwell. As exosomes passed micromagnets, the high gradient fields induced strong magnetophoretic forces leading to their capture. Because the high gradient fields generated via micromagnets are a near-field effect, preferential accumulation of exosome upon micromagnets occurred naturally, leading to patterning (Figure 5).

SUMMARY

This manuscript presents a novel micromagnet fabrication technique and microchip architecture demonstrated for the efficient capture and patterning of magnetically tagged exosomes. Fabrication involves laser-ablation based patterning, which has demonstrated microscale resolution (<50 µm), over large areas (>in^2), with rapid throughput (400 mm/s). Through integrated CFD and magnetostatic simulations we have optimized micromagnet unit cell geometry to maximize capture area ratios. Lastly, when applied within proof-of-concept exosome capture experiments, we demonstrated capture and integrated patterning upon micromagnets directly from undiluted plasma. Future studies of this device will be to benchmark capture efficiency to current state-of-the art systems and establish a standard curve within exosome standards and

buffer solutions to correlate fluorescent intensity to exosomes concentration.

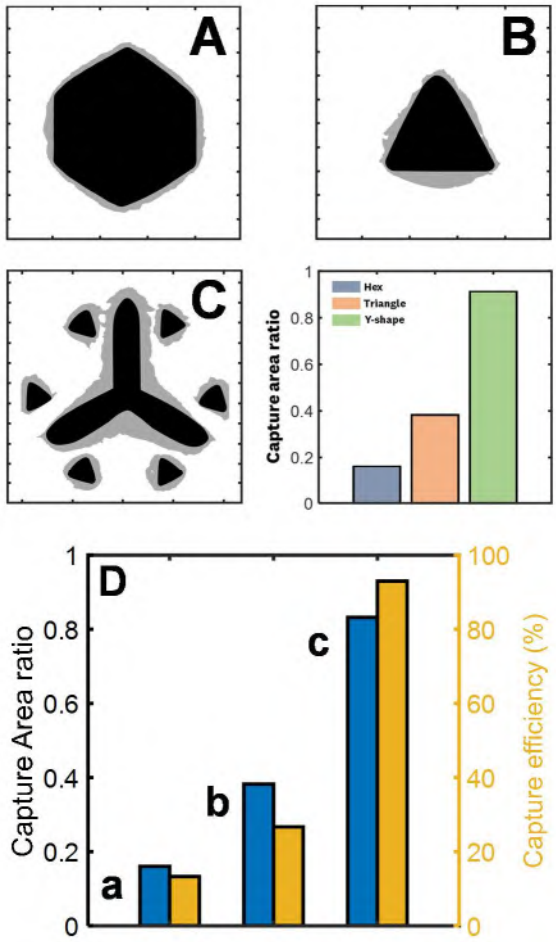

Figure 4: Modeling of capture efficiency via capture area ratio. A-C) Hexagonal, triangle, and Y-shape micromagnet elements, showing capture area ratio for each. D) Shows how correlation between capture area and overall capture efficiency as predicted by the developed computational model.

DISCUSSION

Exosomes have arisen as important biological molecules with intriguing applications within diagnostics and therapeutics. To date, however, their isolation from biologically relevant fluids has remained a challenge which has limited their clinical utility. Though a myriad of devices and techniques have been presented, often these systems require a significant amount of sample preparation, involve complex equipment or manual processing, and are not suitable for clinical integration. Though a select example was presented herein, we foresee this approach having applications within exosome-based diagnostics and rapid sample preparation for molecular analysis, and one that could be readily adapted for profiling or drug loading studies.

ACKNOWLEDGEMENTS

We would like to acknowledge the Dartmouth Innovations Accelerator for Cancer (DIAC) and Magnuson Center for Entrepreneurship for supporting this project. We would also like to extend our sincerest thanks to Ann Lavanway for assistance with confocal microscopy.

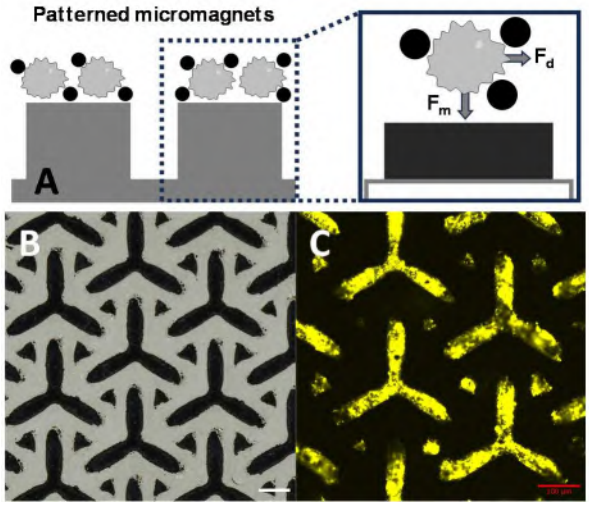

Figure 5: Magnetic capture mechanism and microchip-based exosome capture from plasma. A) Schematic highlighting the mechanism of exosome capture by fluid-pervasive micromagnets. B) Optical microscope image of optimized micromagnets. C) Captured and patterned DiD membrane-stained exosomes upon micromagnets. Scale bars are 100 µm.

REFERENCES

[1] R. Kalluri and V. S. LeBleu, "The biology, function, and biomedical applications of exosomes," *Science (1979)*, vol. 367, no. 6478, Feb. 2020, doi: 10.1126/science.aau6977.

[2] P. Li, M. Kaslan, S. H. Lee, J. Yao, and Z. Gao, "Progress in Exosome Isolation Techniques.," *Theranostics*, vol. 7, no. 3, pp. 789–804, 2017, doi: 10.7150/thno.18133.

[3] P. Zhang *et al.*, "Ultrasensitive detection of circulating exosomes with a 3D-nanopatterned microfluidic chip," *Nat Biomed Eng*, vol. 3, no. 6, pp. 438–451, Jun. 2019, doi: 10.1038/S41551-019-0356-9.

[4] J. C. Contreras-Naranjo, H.-J. Wu, and V. M. Ugaz, "Microfluidics for exosome isolation and analysis: enabling liquid biopsy for personalized medicine.," *Lab Chip*, vol. 17, no. 21, pp. 3558–3577, 2017, doi: 10.1039/c7lc00592j.

[5] E. Reátegui *et al.*, "Engineered nanointerfaces for microfluidic isolation and molecular profiling of tumor-specific extracellular vesicles," *Nat Commun*, vol. 9, no. 1, 2018, doi: 10.1038/s41467-017-02261-1.

[6] P. Zhang, M. He, and Y. Zeng, "Ultrasensitive microfluidic analysis of circulating exosomes using a nanostructured graphene oxide/polydopamine coating," *Lab Chip*, vol. 16, no. 16, pp. 3033–3042, Aug. 2016, doi: 10.1039/C6LC00279J.

[7] E. P. Furlani, "Analysis of particle transport in a magnetophoretic microsystem," *J Appl Phys*, vol. 99, no. 2, p. 024912, Jan. 2006, doi: 10.1063/1.2164531.

CONTACT

*John X.J. Zhang, john.zhang@dartmouth.edu